AIP Journal of Applied Physics

Coupling effect combined with incident polarization to modulate double split-ring-resonator in terahertz frequency range

Mei Zhu, Yu-Sheng Lin, and Chengkuo Lee

Citation: Journal of Applied Physics **116**, 173106 (2014); doi: 10.1063/1.4901062
View online: http://dx.doi.org/10.1063/1.4901062
View Table of Contents: http://scitation.aip.org/content/aip/journal/jap/116/17?ver=pdfcov
Published by the AIP Publishing

Coupling effect combined with incident polarization to modulate double split-ring-resonator in terahertz frequency range

Mei Zhu, Yu-Sheng Lin, and Chengkuo Lee[a)]
Department of Electrical and Computer Engineering, National University of Singapore, 4 Engineering Drive 3, Singapore 117581, Singapore

(Received 3 July 2014; accepted 24 October 2014; published online 5 November 2014)

This work examines the coupling effect in concentric double split-ring-resonator devices in terahertz (THz) range when the inner ring changes its relative orientation to the outer ring. Through detailed analysis on the simulation results of surface current and electrical field distributions, we look into the changes of inductance and capacitance in the system caused by structural layouts, and present a set of coherent theory that is solely rooted in the inductance-capacitance circuit analogy to systematically account for the resonance change. Such coupling effect combined with polarization of the incident wave is further explored to demonstrate continuous modulation of THz resonances. A variation range of transmission intensity from 20% to 80% has been successfully achieved. These experimental results demonstrate the promise of realizing future tunable THz filters by means of rotating sub-structures of the device only. © *2014 AIP Publishing LLC*.
[http://dx.doi.org/10.1063/1.4901062]

I. INTRODUCTION

Recently, great research interests have been devoted to the development of metamaterials for their unique optical properties such as negative refractive indices[1] and attractive applications in super lens,[2] cloaking,[3] sensing,[4] and perfect absorption.[5] Metamaterials consist of sub-wavelength metallic structures, which are able to support resonances. Among these structures, split ring resonators (SRRs)[6] are one the most prominent examples. Both single[7,8] and double SRRs (DSRRs)[1,8,9] have been used in early works as building blocks to construct metamaterials experimentally. In recent researches, SRRs are still among the favorite structures to build metamaterials for various purposes. For example, single SRRs were used in the study of resonance enhancement aided by liquid crystals and indium tin oxide interfaces;[10] DSRR devices were used to study the relationship between resonant frequency and various design parameters;[11] both single and double SRRs have seen applications in tunable metamaterials by means of microelectromechanical systems (MEMS) technologies, either for in-plane tuning[12,13] or out-of-plane tuning;[14–18] their use has also extended to flexible substrates for a variety of applications.[19–22]

Meanwhile, scientists have been studying the resonances of DSRR devices as a result of coupling between the consisting single SRRs. Smith *et al*. first pointed out that the small gap between the two rings increased capacitance of the system and thus reduced the resonant frequency.[9] This shrewd observation was later validated by Linden's group when they proposed the analogy between a conventional inductor-capacitor (LC) circuit and SRRs, and argued that the LC resonant frequency of the metamaterial can be calculated as

$$\omega_{LC} = \sqrt{LC}, \tag{1}$$

where L is the inductance and C is the capacitance of the structures.[7] In the past decade, researchers have looked at the coupling of two identical SRRs when they are placed next to each other[23] on the same plane or stacked on top of each other in two parallel planes.[24,25] They have also looked at coupling between two concentric SRRs, each with a gap situated oppositely.[26–28] The coupling effect was understood by looking at the alignment of electric and magnetic dipolar moments[23,24,26] of individual SRRs or as a result of interaction between the plasmons of individual SRRs.[25,28]

However, when investigating the resonant frequency shift, the previous work on the coupling effect of DSRRs seldom took the LC circuit perspective, with the only exception being Giessen's report in 2007.[27] In this work, they made an attempt to explain the two reflectance peaks in the DSRR spectrum. They identified that these two were due to the LC resonances in the outer and inner rings, respectively. But their theory was only able to account for some of the observations, most of which were changes associated with the low-frequency resonance. When trying to explain the red shift of the second resonance in the DSRR's spectrum, Giessen *et al*. admitted that the result was counter-intuitive and more investigation was needed. On the other hand, many of the previous work on planar DSRRs (including Giessen's) focused mainly on the case when the two SRRs are positioned oppositely.[26,27,29] Notably, however, it was also Giessen's group who later took the initiative to examine the case when the two SRRs were oriented in the same direction. In this work, they based their theory on plasmon hybridization. But as they studied individual structures instead of metamaterial devices comprising periodic DSRRs, they did not discuss the devices' spectra. Consequently, they concluded that relative orientation of individual SRRs was not important in their discussion.[28]

[a)]Author to whom correspondence should be addressed. Electronic mail: elelc@nus.edu.sg.

Based on the LC circuit model proposed by Linden's group,[7] this paper takes on a systematic and coherent approach to understand the coupling effect in square DSRRs with the inner ring rotating 0°, 90°, and 180° with respect to the outer one. We examine the frequency shift in DSRR's spectrum as compared to individual single SRRs' solely from the LC-circuit point of view, and present detailed simulation and experimental results to give account for both the resonant frequency shift and resonant strength change for all three structural layouts with different inner ring orientations. Last but not least, our theory was further explored to offer another mechanism for tuning resonance of metamaterial devices. This extends modulation of THz transmission beyond via electrical[30] and optical[31,32] means, and adds to the knowledge of THz filter and switch designs.

II. COUPLING EFFECT IN SQUARE DSRR DEVICES

To understand the coupling effect in DSRRs, five metamaterial devices (Devices 1 to 5) were fabricated on quartz substrates. The fabrication process started by coating photoresist AZ1512 on the substrate surface, and followed by defining complementary metamaterial patterns via photolithography. A 200 nm thick aluminum (Al) layer was then thermally evaporated onto the photoresist patterns. Finally, after a lift-off step, various single and double SRR patterns were obtained as shown in Fig. 1. Devices 3 to 5 are DSRRs that consist of big and small rings of the same dimensions as Devices 1 and 2, respectively. The outer side lengths, a, of the big ring and small ring are 88 μm and 48 μm, respectively. The line widths, w, and gap widths, d, of the two rings are all 12 μm. As illustrated in Fig. 1, the difference of Devices 3 to 5 lies in that the inner SRR rotates from 0° to 90° and then to 180° with respect to the outer SRR. For all five devices, the lattice constant is kept at 100 μm.

The transmission spectra of the devices were measured with the incident wave polarized along the gap in the big ring (or along the gap in the small ring for Device 2) in the frequency range of 0.3 THz to 1.1 THz. Numerical simulations using commercial software Lumerical finite-difference time-domain (FDTD) were first performed to calculate the transmission spectra and the electromagnetic field distributions corresponding to the resonances with normally incident THz waves. We also characterized the correlation between carrier excitations and incident electromagnetic waves of the devices using a commercial FDTD solver, CST Microwave Studio™ to obtain surface current plots at resonant frequencies.

The simulated and measured spectra of the five devices are presented in Fig. 2 with good agreement. We can see there are altogether three resonances in the frequency of interest, at about 0.35, 0.7, and 1.0 THz, respectively, for Devices 3 to 5. The resonances at about 0.35 and 1.0 THz are also evident in Device 1, whereas resonance at 0.7 THz is the only dip in Device 2's spectrum. (There is also one more resonance for Device 2 at higher frequency, not shown.) Previous research on planar SRR-based THz metamaterials have pointed out two main resonances. One is the low frequency resonance caused by oscillating currents in the SRR loops and charge accumulation at the gap, and is, therefore, called an LC resonance; the other is at higher frequency caused by interactions between the SRR sides or components parallel to the incident electric field, and is called a dipole resonance.[8,33–35] From here on, this paper will only discuss the LC resonances, i.e., the resonances at about 0.35 THz and 0.7 THz. For Devices 3 to 5, these two will also be referred to as the first and the second resonances, respectively, hereafter.

A. Coupling effect when inner SRR rotates 0° and 180°

In Fig. 2, the results are suggestive to show that the first resonance is mainly due to the LC resonance excited in the big ring, while the second is due to that in the small ring. Meanwhile, the difference in spectra can also be observed as a result of the different configurations of the DSRRs. Here,

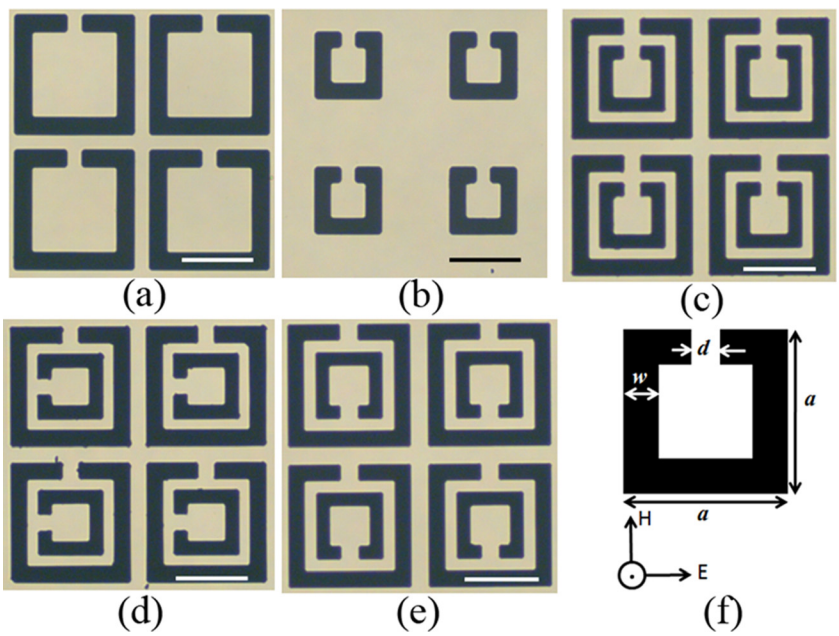

FIG. 1. (a)–(e) Microscopic images of Devices 1 to 5 (using transmitted light). The scale bar in each image is 500 μm. (f) Illustration of SRR dimensions and the incident fields.

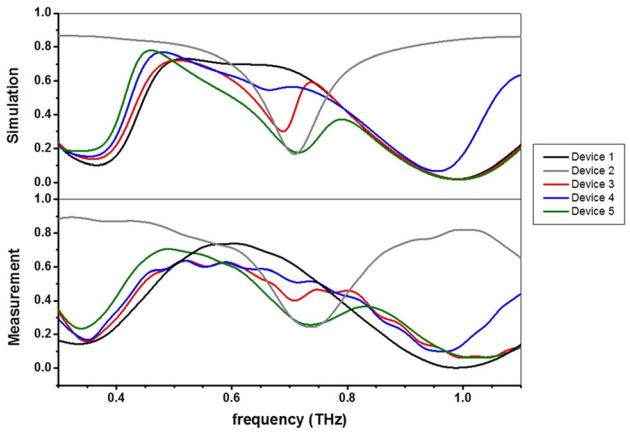

FIG. 2. Simulated and measured spectra of Devices 1 to 5 in the range of 0.3 to 1.1 THz.

we discuss Devices 1, 2, 3, and 5 first, for in these cases, the polarization of the incident wave is always along the gaps of the SRRs. In Fig. 2, the first resonances of Devices 1, 3, and 5 exhibited small difference in terms of transmission intensity and resonant frequency, while the discrepancies of the second resonance of Devices 2, 3, and 5 are much more phenomenal. For a complete understanding of coupling effect in Devices 3 and 5 at both resonances, the simulated surface currents and electrical field distributions along the polarization of the incident wave were presented in Figure 3. Evidenced by the large circulating currents, which are characteristic to LC resonance,[36] we confirm that both resonances are LC resonance, and the first is mainly excited in the outer ring, while the second occurred in the inner ring.

From the plots of normal (along x-direction) electrical field distributions, we deduced polarity of the charges accumulated at the two sides of the gaps (along y-direction), both within each split ring and between the outer and the inner ones. More specifically, if the normal field points outward from the surface, the charges are positive; otherwise if it points into the surface, negative surface charges are indicated. The signs are labeled in Figs. 3(a) to 3(c), to facilitate better understanding of the obvious coupling between the two split rings in these figures. With the current plots and electrical field distributions in Figure 3, we then derived the circuit models for all the four cases (Fig. 4). In Fig. 3(c), as the current in the outer SRR is not circulating as in all other cases, but rather breaks into 3 segments with reverse directions, L1, L2, and L3 is thus used to represent the inductance of the three segments of the outer SRR in which these reverse currents flow. For Fig. 3(d), the electrical field plots show that the electrical field in the outer ring and the inner ring has a 90° phase difference. This indicates that the inner ring is excited independently of the outer ring. Hence, the circuit model shows the inductance L and capacitance C of the inner ring only. This is also the reason why at the second resonance, Devices 2 and 5 showed minimal difference in terms of transmission intensity and resonant frequency.

To get the equivalent circuit of the other 3 cases, the mutual inductance between the outer and inner rings is considered and denoted as M in Fig. 4. Assuming all the flux in the inner ring passes through the outer ring and vice versa, the mutual inductance can be calculated as

$$M = \sqrt{L_{out}L_{in}}, \tag{2}$$

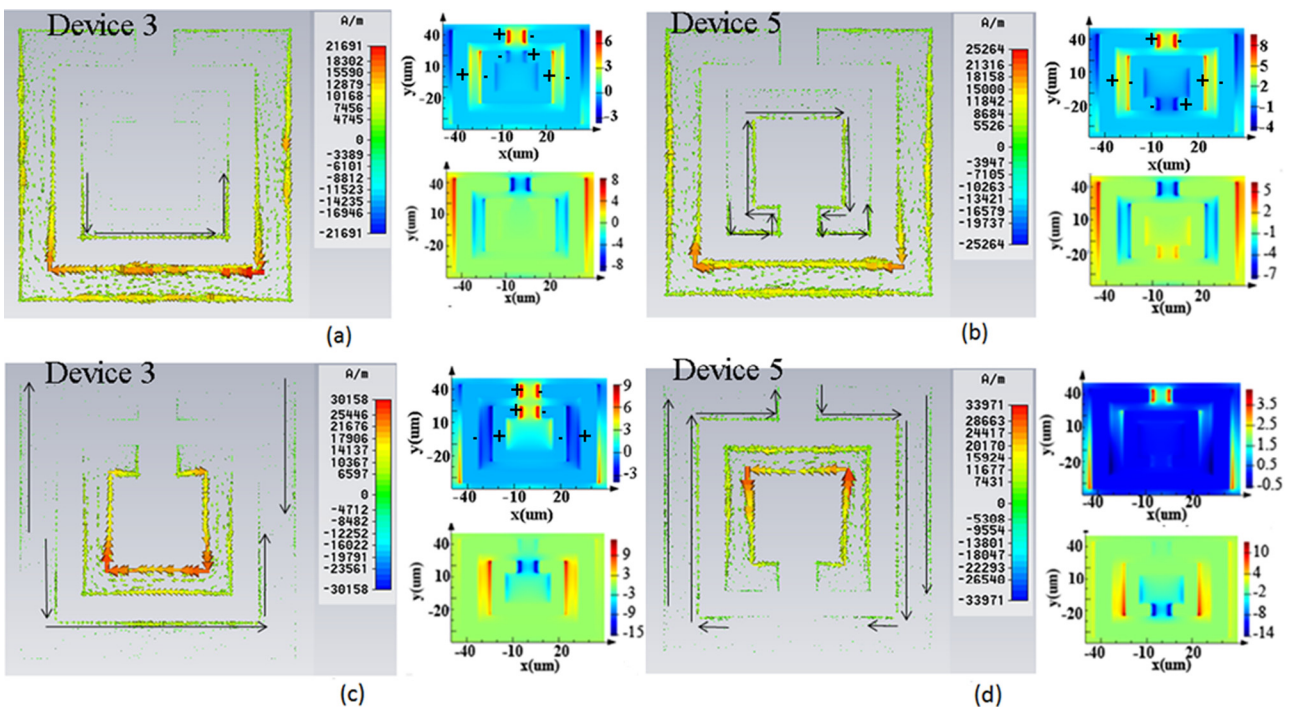

FIG. 3. Surface current (left) and electrical field distributions along the x-direction (right) in (a) Device 3 and (b) Device 5 at first resonance, and in (c) Device 3 and (d) Device 5 at the second resonance, respectively. The black arrows in the current plots aid to better visualize directions of small current. The electrical field plots show the real part (top) and imaginary part (bottom), separately. The + and − signs in the plots indicate the polarity of charges accumulated at the two sides of the gaps.

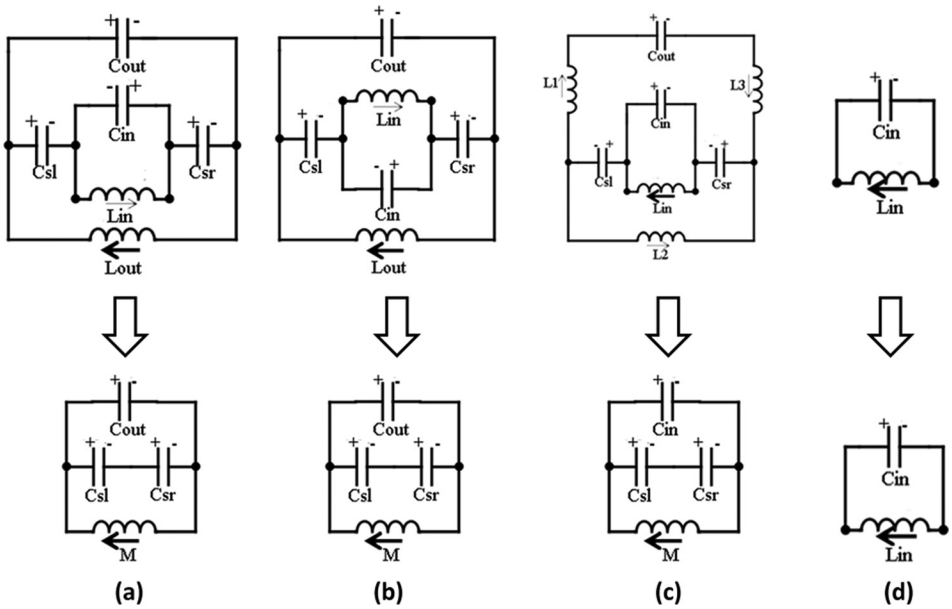

FIG. 4. Circuit models and the corresponding equivalent circuits for (a) Device 3 and (b) Device 5 at first resonance and for (c) Device 3 and (d) Device 5 at the second resonance, respectively. The thick and thin arrows indicate the directions and magnitudes of currents in the paths, with a thicker arrow indicating a larger current. L1, L2, and L3 in (c) represent the inductance of the three segments of the outer SRR in which currents of reverse directions flow.

where L_{out} and L_{in} stand for the inductance of the outer and inner rings, respectively. As the inductance of a single loop wire is proportional to its loop area, L_{out} is larger than L_{in}. Hence

$$L_{in} < M < L_{out}. \tag{3}$$

Then to get the equivalent capacitance, the small currents in the circuit models are neglected (the inductors are considered as negligible voltage sources, i.e., short circuit). With the equivalent circuit presented in Fig. 4, the effective capacitance can be calculated as

$$C_{eff} = C_{out} + \frac{C_{sl}C_{sr}}{C_{sl} + C_{sr}} \tag{4}$$

at the first resonance and

$$C_{eff} = C_{in} + \frac{C_{sl}C_{sr}}{C_{sl} + C_{sr}}. \tag{5}$$

At the second resonance for Device 3, where C_{out} and C_{in} are the capacitance of the outer and inner rings, respectively, while C_{sl} and C_{sr} are the capacitance between the left and right arms of the two rings, respectively. C_{sl} and C_{sr} can be calculated as

$$C_{sl} = C_{sr} = \frac{C_0}{2}, \tag{6}$$

where C_0 stands for the total capacitance between the two rings.

Equations (2) and (4) show that at the first resonance, in both Devices 3 and 5, the effective inductance reduces and the capacitance increases, as compared to Device 1. According to Eq. (1), the canceling effect of these two changes attributes to the negligible resonant frequency shift at the first resonant. On the other hand, for Device 3 at the second resonance, the effective inductance and capacitance both increase as compared to Device 2, therefore, the spectrum exhibits a red shift.

The transmission intensity is affected by surface current distributions. At the first resonance, Figures 3(a) and 3(b) show that besides the large current flowing in the outer ring, in Device 3, the current in the inner ring mainly flows along its outer rim, while it is along the inner rim in Device 5. This essentially reduces the area in which the magnetic flux is concentrated. As a result, Device 5 has the smallest effective field area, while Device 1 has the largest one. In other words, more energy from the incident wave can couple into Device 1 than Device 5. Therefore, at the first resonance, Device 1 shows the strongest resonance strength, and Device 5 shows the weakest. At the second resonance in Device 3, although the effective filed area remains the same as Device 2, the resonant frequency in this case is smaller than that of the inner ring alone. This means less energy can couple into the inner ring, which is the primary resonator. On the other hand, the current induced in the outer ring is not in a circular fashion, and thus does not contribute to the LC resonance at this frequency. These lead to the fact that Device 3 has a significantly weaker resonance than Device 2.

B. Modulation of the second resonance when inner SRR rotates 90°

For the transmission spectrum of Device 4 shown in Fig. 2, a small non-distinct dip at about 0.67 THz can be taken for its second resonance. To understand this, the surface current at the second resonance is examined for Devices 4 and 2 (Fig. 5). In Fig. 5(a), with the incident light polarized perpendicular to the gap-bearing side of the small SRR, if the outer ring is not present, the inner ring is symmetric about the polarization. As a result, the polarization current can only flow along the two arms of the SRR and no circulating current can be formed.[36] In Device 4, with the presence of the outer ring, the structure symmetry is broken and, consequently, a circulating current is induced in the inner ring; an LC resonance is excited. Nevertheless, the main resonating structure, i.e., the inner SRR, is still symmetric about the polarization; light energy cannot efficiently couple into the

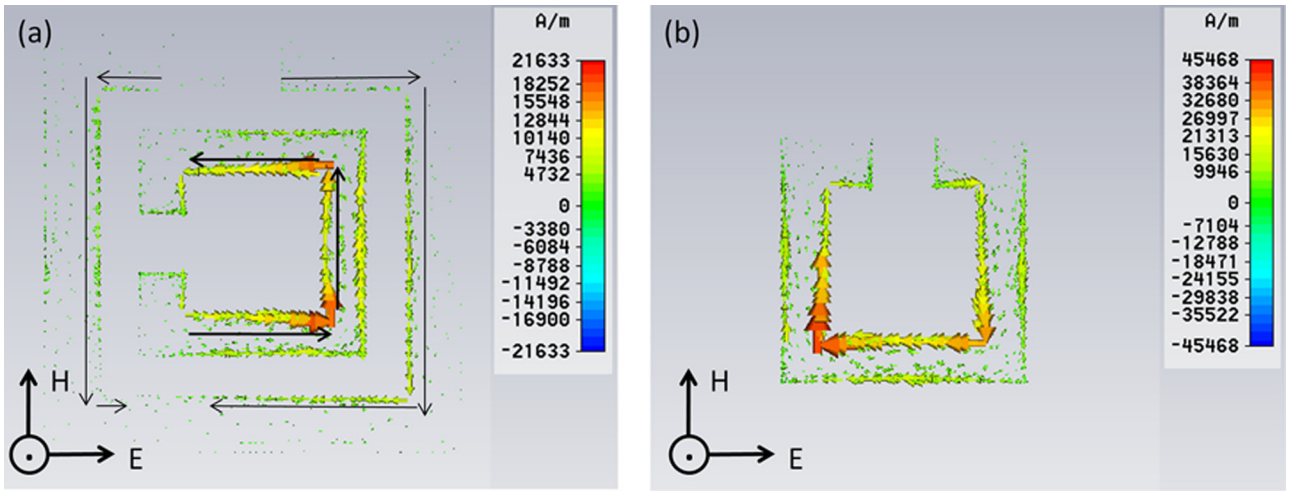

FIG. 5. Surface current distributions at the second resonance in (a) Device 4 and (b) Device 2.

device, evidenced by the smaller current in Device 4 than Device 2. This leads to a weaker resonance in Device 4 as compared to Devices 2, 3, and 5.

III. CONTINUOUSLY MODULATE THE RESONANT STRENGTH IN CIRCULAR DSRR

The investigation in Sec. II highlights the fact that the resonant strength of a DSRR device can be modulated by simply changing the relative orientation of its consisting single SRRs. This potentially brings forth a new way to modulate THz transmission. It can be very useful in future filter designs as this method requires no change of the device materials or any substrate property alteration, as compared to previously reported means.[30–32,37] In order to fully exploit the modulation of the second resonance, we proposed the idea of a concentric circular DSRR device of which the inner ring can rotate from 0° to 180° continuously. In this way, the strength of the second resonance can be modulated from the weakest to the strongest in a continuous fashion. With the development of MEMS technology, such a device may be realized with further efforts. In this work, for the purpose of demonstration of concept only, we fabricated Devices A to E as shown in Figs. 6(a) to 6(e), which consists of circular DSRRs with the inner ring rotating from 0° to 180° at a step of 45°. The outer SRR has an outer diameter a of 100 μm, inner diameter b of 76 μm, and a gap width d of 12 μm, while a, b, and d of the inner SRR are 60, 40, and 12 μm, respectively, as illustrated in Fig. 6(f). The lattice constant for all devices are 114 μm. The well-matched simulated and measured transmission spectra of these devices are shown in Fig. 7. At the second resonance, the variation range of transmission intensity was as large as 60%, modulated from 20% to 80%. These experimental results opened up broad arena for various optical applications arising from rotating the inner ring or outer ring, such as tunable MEMS-based THz filters and switches.

IV. CONCLUSIONS

In conclusion, this paper presented a holistic and systematic investigation of the coupling effect in concentric DSRRs. Through both simulation and experimental efforts, it examined the changes in resonant frequency and strength

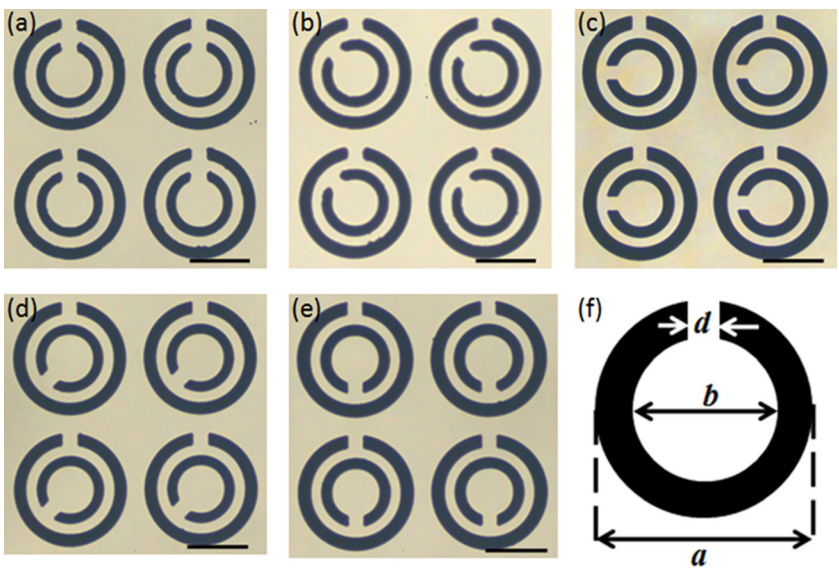

FIG. 6. (a)–(e) Microscopic images of Devices A to E (using transmitted light), of which the concentric outer rings and inner rings are of the same dimensions except that the inner ring rotates from 0° to 180° at a step of 45°. The scale bars in all pictures are 50 μm. (f) Illustration of outer and inner ring parameters.

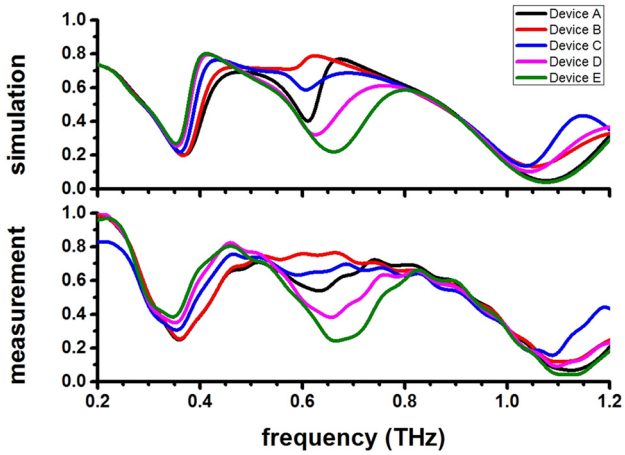

FIG. 7. Simulated and measured spectra of Devices A to E in the range of 0.2 to 1.2 THz.

of DSRR devices as a result of different relative orientations of the two consisting single SRRs. With the inner ring rotating from 0°, 90°, and 180°, this work simulated surface current and electrical field distributions in all cases with the aim to find the change in inductance and capacitance. We proposed a set of theory that was solely rooted in the LC circuit analogy to give coherent account for the resulting THz spectra of the DSRR devices. This work provides greater momentum to current research in coupling effect, as it not only focused on structure layouts that have not been investigated systematically before, but also offered a set of consistent theory from a perspective that has rarely been taken in this area.

With the principles being fully understood, the demonstration with a set of circular DSRR devices pointed out new direction for future designs of optical applications. As an advantage over square DSRRs, circular DSRR devices are capable of continuous tuning. We demonstrated a modulation of transmission level from 20% to 80% with both simulation and experimental results. This promises future tunable THz filter designs based on rotating sub-structures only.

ACKNOWLEDGMENTS

This work was supported by Grants from AcRF Tier 2—MOE 2012-T2-2-154 (R-263-000-A59-112) at National University of Singapore and the National Research Foundation (NRF) CRP Project "Self-Powered Body Sensor Network for Disease Management and Prevention Oriented Healthcare" (R-263-000-A27-281). The authors also want to thank Institute of Materials Research and Engineering (IMRE), a Research Institute of the Agency for Science, Technology and Research (A*STAR), Singapore, for their support of the THz spectroscopy used in this work.

[1]R. Shelby, D. Smith, and S. Schultz, "Experimental verification of a negative index of refraction," Science **292**, 77–79 (2001).
[2]N. Fang, H. Lee, C. Sun, and X. Zhang, "Sub-diffraction-limited optical imaging with a silver superlens," Science **308**, 534–537(2005).
[3]J. Pendry, D. Schurig, and D. Smith, "Controlling electromagnetic fields," Science **312**, 1780–1782 (2006).
[4]Z. G. Dong, H. Liu, J. X. Cao, T. Li, S. M. Wang, S. N. Zhu, and X. Zhang, "Enhanced sensing performance by the plasmonic analog of electromagnetically induced transparency in active metamaterials," Appl. Phys. Lett. **97**, 114101 (2010).
[5]K. Aydin, V. E. Ferry, R. M. Briggs, and H. A. Atwater, "Broadband polarization-independent resonant light absorption using ultrathin plasmonic super absorbers," Nat. Commun. **2**, 517 (2011).
[6]J. B. Pendry, A. J. Holden, D. J. Robbins, and W. J. Stewart, "Magnetism from conductors and enhanced nonlinear phenomena," IEEE Trans. Microwave Theory Tech. **47**, 2075–2084 (1999).
[7]S. Linden, C. Enkrich, M. Wegener, J. Zhou, T. Koschny, and C. M. Soukoulis, "Magnetic response of metamaterials at 100 terahertz," Science **306**, 1351–1353 (2004).
[8]M. Kafesaki, T. Koschny, R. S. Penciu, T. F. Gundogdu, E. N. Economou, and C. M. Soukoulis, "Left-handed metamaterials: Detailed numerical studies of the transmission properties," J. Opt. A: Pure Appl. Opt. **7**, S12–S22 (2005).
[9]D. R. Smith, W. J. Padilla, D. C. Vier, S. C. Nemat-Nasser, and S. Schultz, "Composite medium with simultaneously negative permeability and permittivity," Phys. Rev. Lett. **84**, 4184–4187 (2000).
[10]Z. Liu, C. Huang, H. Liu, X. Zhang, and C. Lee, "Resonance enhancement of terahertz metamaterials by liquid crystals/indium tin oxide interfaces," Opt. Express **21**, 6519–6525 (2013).
[11]A. K. Azad, J. Dai, and W. Zhang, "Transmission properties of terahertz pulses through subwavelength double split-ring resonators," Opt. Lett. **31**, 634–636 (2006).
[12]W. M. Zhu, A. Q. Liu, X. M. Zhang, D. P. Tsai, T. Bourouina, J. H. Teng, X. H. Zhang, H. C. Guo, H. Tanoto, T. Mei, G. Q. Lo, and D. L. Kwong, "Switchable magnetic metamaterials using micromachining processes," Adv. Mater. **23**, 1792–1796 (2011).
[13]Y. H. Fu, A. Q. Liu, W. M. Zhu, X. M. Zhang, D. P. Tsai, J. B. Zhang, T. Mei, J. F. Tao, H. C. Guo, X. H. Zhang, J. H. Teng, N. I. Zheludev, G. Q. Lo, and D. L. Kwong, "A micromachined reconfigurable metamaterial via reconfiguration of asymmetric split-ring resonators," Adv. Funct. Mater. **21**, 3589–3594 (2011).
[14]Y. Lin, Y. Qian, F. Ma, Z. Liu, P. Kropelnicki, and C. Lee, "Development of stress-induced curved actuators for a tunable THz filter based on double split ring resonators," Appl. Phys. Lett. **102**, 111908 (2013).
[15]M. Ma, Y. Qian, Y. Lin, H. Liu, X. Zhang, Z. Liu, J. M. Tsai, and C. Lee, "Polarization-sensitive microelectromechanical systems based tunable terahertz metamaterials using three dimensional electric split-ring resonator arrays," Appl. Phys. Lett. **102**, 161912 (2013).
[16]Y. Lin, F. Ma, and C. Lee, "Three-dimensional movable metamaterials using electric split-ring resonators," Opt. Lett. **38**, 3126–3128 (2013).
[17]H. Tao, A. C. Strikwerda, K. Fan, W. J. Padilla, X. Zhang, and R. D. Averitt, "Reconfigurable terahertz metamaterials," Phys. Rev. Lett. **103**, 147401 (2009).
[18]Z. Han, H. Fujita, and H. Toshiyoshi, "Electrostatically tunable MEMS THz metamaterials based on DC/RF decoupled split-ring resonator arrays," in *Proceedings of 2012 International Conference on Optical MEMS and Nanophotonics (OMN), Banff, Canada*, 6–9 August 2012, pp. 27–28.
[19]H. Tao, J. J. Amsden, A. C. Strikwerda, K. Fan, D. L. Kaplan, X. Zhang, R. D. Averitt, and F. G. Omenetto, "Metamaterial silk composites at terahertz frequencies," Adv. Mater. **22**, 3527–3531 (2010).
[20]H. Tao, L. R. Chieffo, M. A. Brenckle, S. M. Siebert, M. Liu, A. C. Strikwerda, K. Fan, D. L. Kaplan, X. Zhang, R. D. Averitt, and F. G. Omenetto, "Metamaterials on paper as a sensing platform," Adv. Mater. **23**, 3197–3201 (2011).
[21]N. R. Han, Z. C. Chen, C. S. Lim, B. Ng, and M. H. Hong, "Broadband multi-layer terahertz metamaterials fabrication and characterization on flexible substrates," Opt. Exp. **19**, 6990–6998 (2011).
[22]K. Fan, A. C. Strikwerda, H. Tao, X. Zhang, and R. D. Averitt, "Stand-up magnetic metamaterials at terahertz frequencies," Opt. Exp. **19**, 12619–12627 (2011).
[23]N. Liu, S. Kaiser, and H. Giessen, "Magnetoinductive and electroinductive coupling in plasmonic metamaterial molecules," Adv. Mater. **20**, 4521–4525 (2008).
[24]N. Liu, H. Liu, S. Zhu, and H. Giessen, "Stereometamaterials," Nat. Photonics **3**, 157–162 (2009).
[25]T. Q. Li, H. Liu, T. Li, S. M. Wang, J. X. Cao, Z. H. Zhu, Z. G. Dong, S. N. Zhu, and X. Zhang, "Suppression of radiation loss by hybridization effect in two coupled split-ring resonators," Phys. Rev. B **80**, 115113 (2009).
[26]J. García-García, F. Martín, J. D. Baena, R. Marqués, and L. Jelinek, "On the resonances and polarizabilities of split ring resonators," J. Appl. Phys. **98**, 033103 (2005).

[27]N. Liu, H. Guo, L. Fu, H. Schweizer, S. Kaiser, and H. Giessen, "Electromagnetic resonances in single and double split-ring resonator metamaterials in the near infrared spectral region," Phys. Status Solidi B **244**, 1251–1255 (2007).
[28]H. Guo, N. Liu, L. Fu, T. P. Meyrath, T. Zentgraf, H. Schweizer, and H. Giessen, "Resonance hybridization in double split-ring resonator metamaterials," Opt. Exp. **15**, 12095–12101 (2007).
[29]A. Bitzer, H. Merbold, A. Thoman, T. Feurer, H. Helm, and M. Walther, "Terahertz near-field imaging of electric and magnetic resonances of a planar metamaterial," Opt. Exp. **17**, 3826–3834 (2009).
[30]H. Chen, W. J. Padilla, H. M. O. Zide, A. C. Gossard, A. J. Taylor, and R. D. Averitt, "Active terahertz metamaterial devices," Nature **444**, 597–600 (2006).
[31]H. Chen, J. F. O'Hara, A. K. Azad, A. J. Taylor, R. D. Averitt, D. B. Shrekenhamer, and W. J. Padilla, "Experimental demonstration of frequency-agile terahertz metamaterials," Nat. Photonics **2**, 295–298 (2008).
[32]C. Wang, D. Kuang, S. Chang, and L. Lin, "A metamaterial terahertz modulator based on complementary planar double-split-ring resonator," Optoelectron. Lett. **9**, 0266–0269 (2013).
[33]W. J. Padilla, A. J. Taylor, C. Highstrete, M. Lee, and R. D. Averitt, "Dynamical electric and magnetic metamaterial response at terahertz frequencies," Phys. Rev. Lett. **96**, 107401 (2006).
[34]G. Dolling, C. Enkrich, M. Wegener, J. F. Zhou, C. M. Soukoulis, and S. Linden, "Cut-wire pairs and plate pairs as magnetic atoms for optical metamaterials," Opt. Lett. **30**, 3198–3200 (2005).
[35]A. K. Azad, A. J. Taylor, E. Smirnova, and J. F. O'Hara, "Characterization and analysis of terahertz metamaterials based on rectangular split-ring resonators," Appl. Phys. Lett. **92**, 011119 (2008).
[36]N. Katsarakis, T. Koschny, M. Kafesaki, E. N. Economou, and C. M. Soukoulis, "Electric coupling to the magnetic resonance of split ring resonators," Appl. Phys. Lett. **84**, 2943 (2004).
[37]R. Singh, E. Smirnova, A. J. Taylor, J. F. O'Hara, and W. Zhang, "Optically thin terahertz metamaterials," Opt. Exp. **16**, 6537–6543 (2008).